

A stable lanthanum hydroxamate metal-organic framework with radical character and electrical conductivity

Yong Yan,^a Ning-Ning Zhang,^b Daniel Fuhrmann,^a Stefan Merker^a and Harald Krautscheid^{*a}

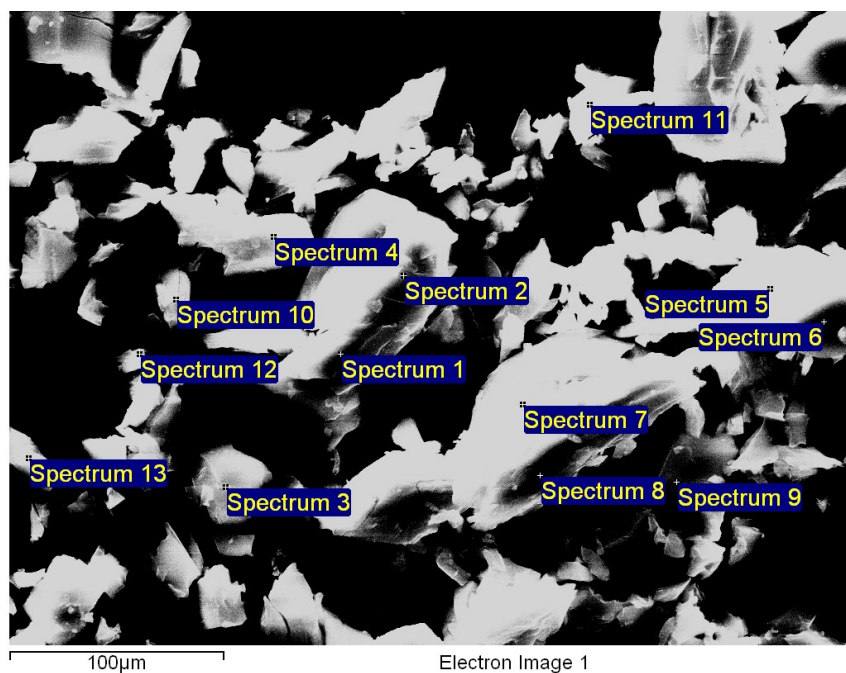
^a Fakultät für Chemie und Mineralogie, Institut für Anorganische Chemie, Universität Leipzig, Johannisallee 29, 04103 Leipzig, Germany.

^b School of Chemistry and Chemical Engineering, Liaocheng University, Liaocheng 252059, P. R. China.

Table S1 Crystal structure data and refinement data for **La-ONDI** and **Sm-ONDI**.

	La-ONDI	Sm-ONDI
Empirical formula	C ₁₇ H _{18.75} N _{2.75} O _{10.75} ClLa* (refinement: C ₁₄ H ₁₂ N ₂ O ₁₀ La)	C ₁₇ H ₁₃ N ₃ O ₈ ClSm* (refinement: C ₁₄ H ₆ N ₂ O ₇ Sm)
moiety formula	C ₁₄ H ₈ LaN ₂ O ₈ , Cl, 2(H ₂ O), 0.75(C ₄ H ₉ NO)	C ₁₄ H ₆ N ₂ O ₇ Sm, Cl, C ₃ H ₇ NO
Formula weight/g·mol ⁻¹	607.96	573.10
Temperature/K	180	180
Crystal system	monoclinic	monoclinic
Space group	<i>C2/c</i>	<i>C2/c</i>
<i>a</i> , Å	19.2116(14)	20.5997(12)
<i>b</i> , Å	14.8074(11)	12.3311(9)
<i>c</i> , Å	8.5126(7)	8.2059(5)
α (deg)	90	90
β (deg)	99.908(6)	95.074(5)
γ (deg)	90	90
<i>V</i> /Å ³	2385.5(3)	2076.3(2)
<i>Z</i>	4	4
λ/Å	1.54186	1.54186
<i>D</i> _{calc} (g cm ⁻³)	1.693	1.833
μ/mm ⁻¹	15.397	22.873
<i>F</i> (000)	1200	1116
Reflections collected	9350	6650
Independent reflections	2257 (R _{int} = 0.0269)	1953 (R _{int} = 0.0418)
Observed refl. [<i>I</i> > 2σ(<i>I</i>)]	2106	1847
Completeness	0.980 (θ _{max} = 70.631)	0.976 (θ _{max} = 70.969)
GOF	1.077	1.060
R ₁ ^a , wR ₂ ^b [<i>I</i> > 2σ(<i>I</i>)]	0.0335, 0.0916	0.0464, 0.1237
R ₁ ^a , wR ₂ ^b (all data)	0.0356, 0.0927	0.0486, 0.1256
CCDC number	2181884	2181885
a) R ₁ = Σ F _o - F _c / Σ F _o ; b) wR ₂ = [Σw(F _o ² -F _c ²) ² / Σw(F _o ²) ²] ^{1/2} *) The SQUEEZE routine (PLATON) ¹ has been applied. Numbers for formula weight, calculated density, absorption coefficient and F(000) correspond to the complete formula. The atoms of disordered solvents and counter ions have not been included in the refinement; a solvent mask was calculated and 246 electrons were found in a volume of 910 Å ³ in one void per unit cell of La-ONDI , which is comparable with the experimental value for 212 electrons (4 Cl and 3 DMA per unit cell). For Sm-ONDI , 236 electrons in a volume of 834 Å ³ may correspond 4 Cl and 4 DMF per unit cell (228 electrons).		

Table S2 Energy-dispersive X-ray spectroscopy (EDX) results of **La-ONDI**. KCl and LaB₆ were used as standard materials.



	Cl		La		Total (100%)
	(weight %)	(atomic %)	(weight %)	(atomic %)	
Spectrum 1	18.63	47.29	81.37	52.71	100.00
Spectrum 2	18.77	47.52	81.23	52.48	100.00
Spectrum 3	15.41	41.65	84.59	58.35	100.00
Spectrum 4	15.34	41.53	84.66	58.47	100.00
Spectrum 5	19.14	48.12	80.86	51.88	100.00
Spectrum 6	15.31	41.46	84.69	58.54	100.00
Spectrum 7	18.60	47.24	81.40	52.76	100.00
Spectrum 8	18.06	46.34	81.94	53.66	100.00
Spectrum 9	16.42	43.50	83.58	56.50	100.00
Spectrum 10	16.10	42.91	83.90	57.09	100.00
Spectrum 11	17.20	44.87	82.80	55.13	100.00
Spectrum 12	16.06	42.84	83.94	57.16	100.00
Spectrum 13	18.83	47.62	81.17	52.38	100.00
average	17.22	44.87	82.78	55.13	100.00

Table S3 Comparison of spin number, estimated percentage of NDI^{•-}, and electrical conductivity of reported NDI^{•-} doped MOFs.

NDI-derived Compounds	Detected spin number	Percentage of NDI ^{•-}	Electrical conductivity
ZnNDI-A ²	7.5×10 ¹⁷ /mg	90%	2×10 ⁻⁷ S/cm (Pellet)
ZnNDI-B ²	5.0×10 ¹⁷ /mg	50%	1×10 ⁻⁹ S/cm (Pellet)
ZnNDI-C ²	2.0×10 ¹⁷ /mg	20%	3×10 ⁻¹⁰ S/cm (Pellet)
PMC-1 ³	N/A	N/A	2.2×10 ⁻³ S/cm (single crystals) 4.5×10 ⁻⁶ S/cm (Pellet)
PMC-2 ⁴	N/A	2%	1.4×10 ⁻⁶ S/cm (single crystals)
La-ONDI-DMA (this work)	1.19×10 ¹⁵ /mg	0.11%	2.1×10 ⁻⁸ S/cm (Pellet)
La-ONDI-DMF (this work)	2.87×10 ¹⁶ /mg	2.79%	2.4×10 ⁻⁶ S/cm (Pellet)
La-ONDI-Catechol (this work)	5.86×10 ¹⁶ /mg	5.69%	5.9×10 ⁻⁶ S/cm (Pellet)

Table S4 Comparison of unit cell parameter of reported Ce(HCOO)₃⁵ and the colorless byproduct formed during syntheses without 18-crown-6.

Cell parameters	reported Ce(HCOO) ₃	colorless byproduct
crystal system	hexagonal	hexagonal
<i>a</i> / Å	10.706(2)	10.726(3)
<i>c</i> / Å	4.1205 (12)	4.1353(11)
<i>V</i> / Å ³	409.01	412.04(18)

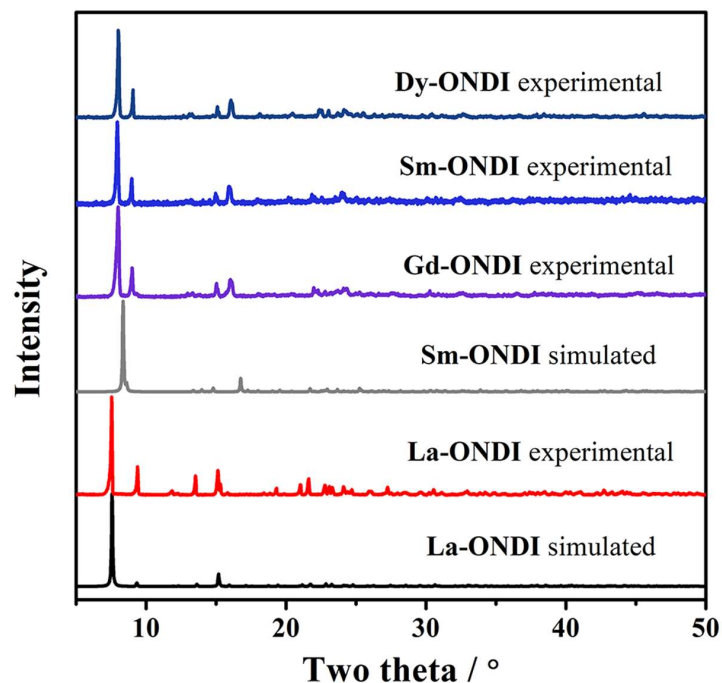


Fig. S1 PXRD patterns of **La-ONDI**, **Sm-ONDI**, **Gd-ONDI**, **Dy-ONDI**. The results of Pawley refinements for **Sm-ONDI**, **Gd-ONDI** and **Dy-ONDI** are given in Fig. S23. In case of **Sm-ONDI**, single crystals were separated from the mixture of products and used for SXRDR.

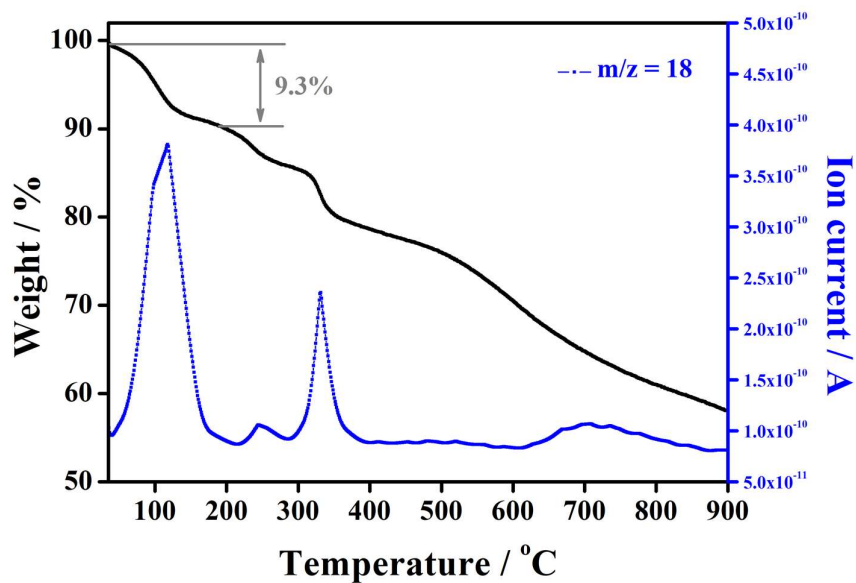


Fig. S2 TG curve and MS signal of $(\text{H}_2\text{O})^+$ ($m/z = 18$) of **La-ONDI**. The weight loss of 9.3 % below 200 °C is assigned to the loss of non-coordinated and coordinated water (calculated value: 9.16 %) in **La-ONDI**.

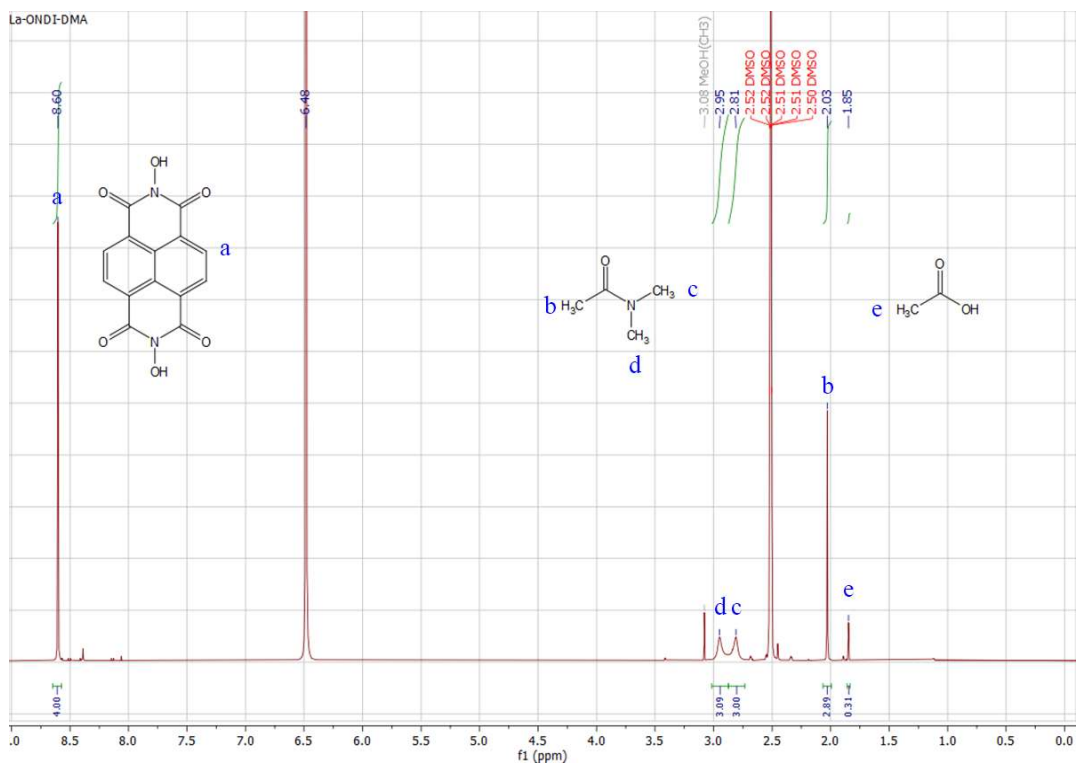


Fig. S3 ^1H NMR spectrum of La-ONDI-DMA dissolved in DMSO- d_6 and DCl (20 wt-% in D_2O). A clear solution was obtained by filtering off (0.45 μm) the yellow precipitate. The proton signal at 1.85 ppm might be due to acetic acid which originates from the hydrolysis of DMA under solvothermal conditions.

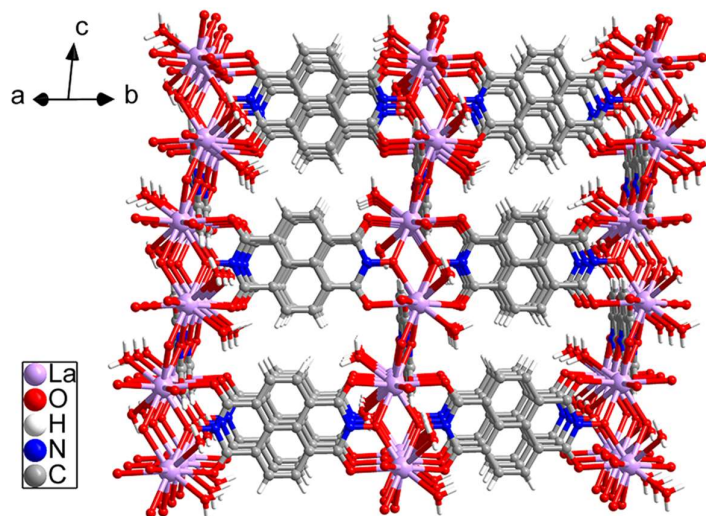


Fig. S4 Fragment of the crystal structure of La-ONDI showing La-O-chains connected by ONDI $^{2-}$ ligands.

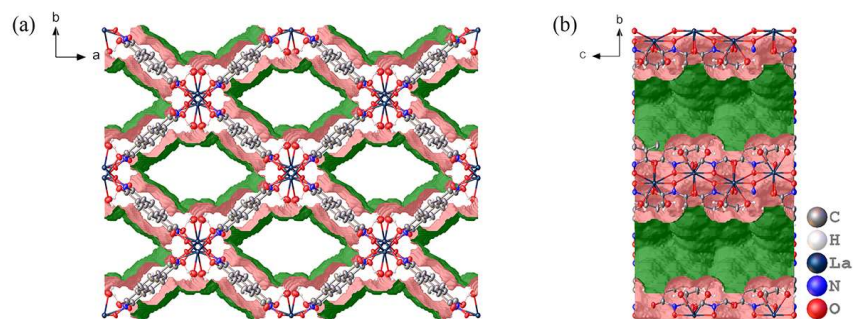


Fig. S5 Representation of solvent accessible voids along the *c* axis (a) and the curvy inner channel along the *a* axis (b) of **La-ONDI**. These pictures were generated by Olex2.⁶

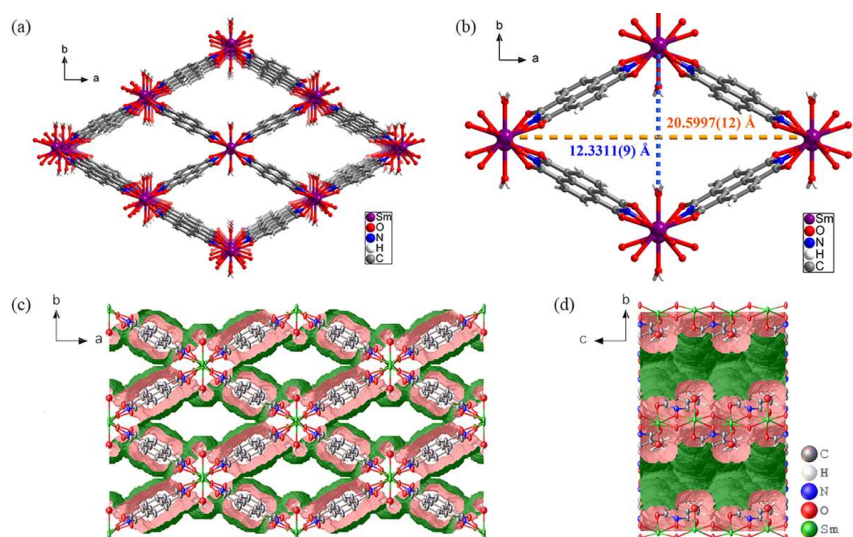


Fig. S6 A view of the porous framework of **Sm-ONDI** along the crystallographic *c* axis (a); an enlarged fragment of the structure of **Sm-ONDI**, the Sm...Sm distances marked with dashed lines correspond to the unit cell axes (b); representation of solvent accessible voids along the *c* axis (c) and the curvy inner channel along the *a* axis (d) in **Sm-ONDI**.

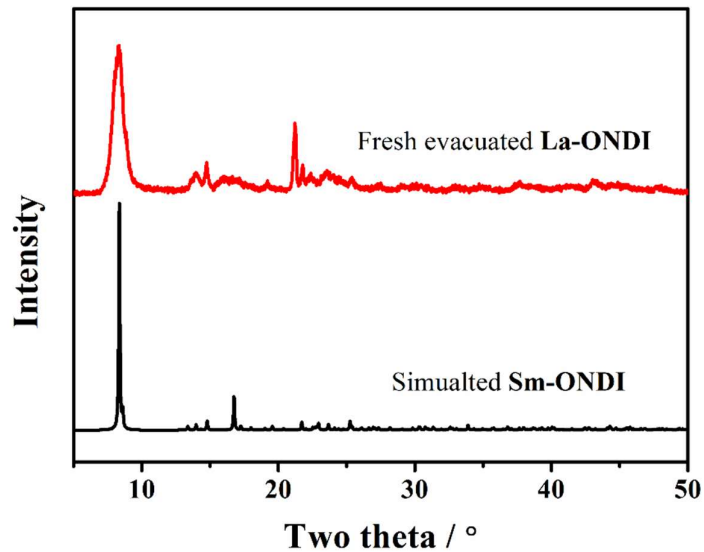


Fig. S7 PXRD pattern of freshly evacuated **La-ONDI** and comparison to the simulated pattern of **Sm-ONDI** based on single crystal data.

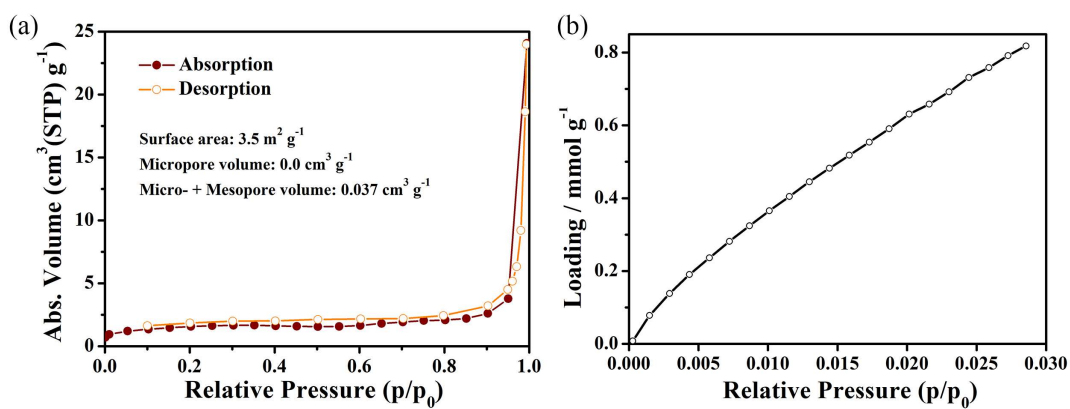


Fig. S8 N_2 adsorption and desorption isotherm (a) and CO_2 adsorption (b) of activated **La-ONDI** at 77 K and 273.15 K, respectively. The results show that **La-ONDI** is nearly non-porous for N_2 and CO_2 , possibly caused by a structural transformation of the initial porous phase during activation.

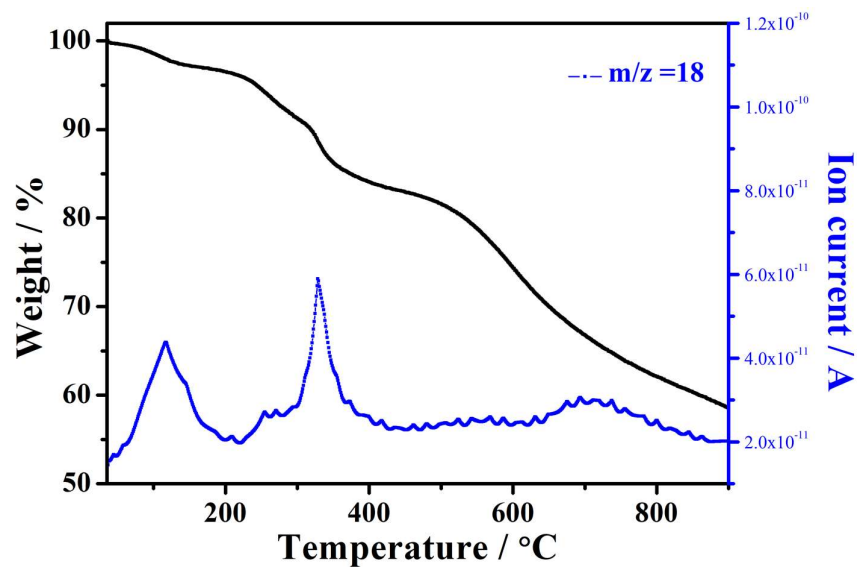


Fig. S9 TG curve and MS signal of $(\text{H}_2\text{O})^+$ ($m/z = 18$) of freshly activated **La-ONDI**. The first weight loss (3 %) should be attributed to the loss of coordinated water (calculated: 6.10 %). The smaller experimental percentage of coordinated water after the activation process implies that coordinated water molecules are only partially lost.

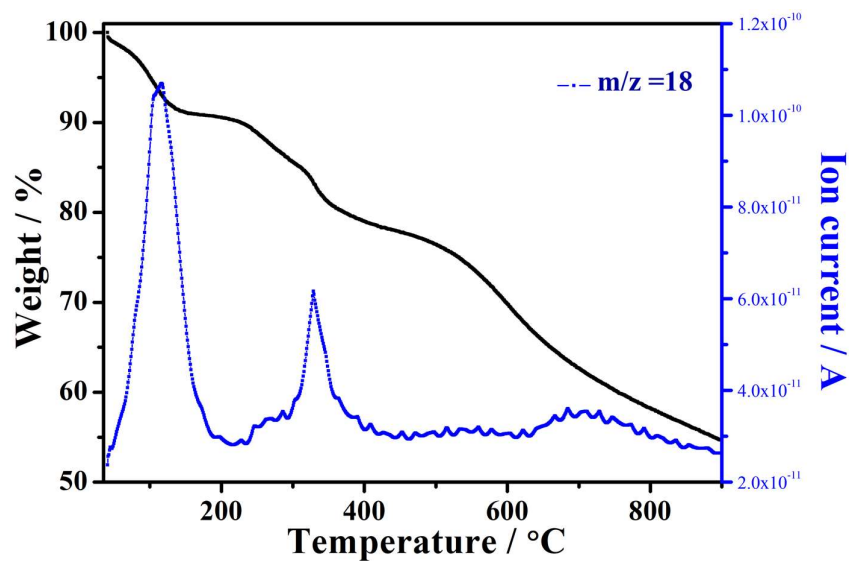


Fig. S10 TG curve and MS signal of $(\text{H}_2\text{O})^+$ ($m/z = 18$) of **La-ONDI** after activation and exposure to air for 6 days. The first weight loss is assigned to water vapor adsorbed during exposure to air.

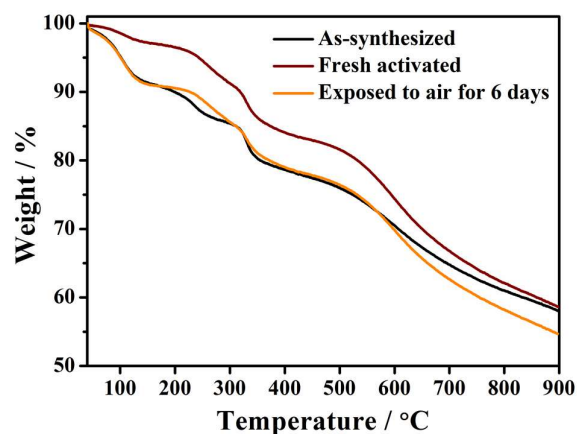


Fig. S11 Comparison of TG curves of as-synthesized La-ONDI, freshly activated La-ONDI, and after exposure to air for 6 days.

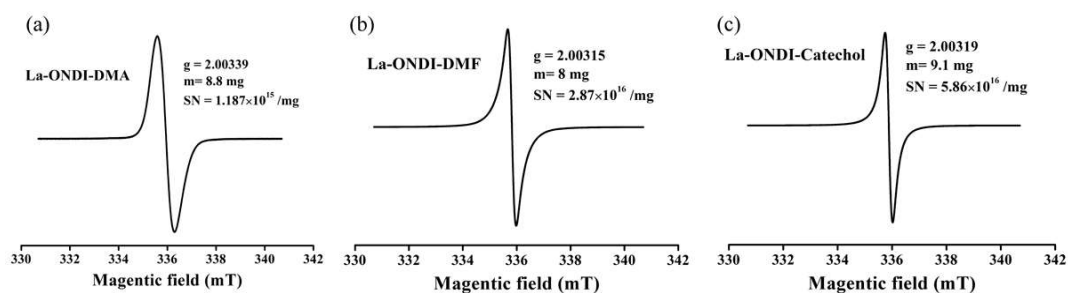


Fig. S12 EPR spectra and spin numbers of La-ONDI-DMA, La-ONDI-DMF and La-ONDI-Catechol. The spin numbers correspond to 0.1%, 2.8% and 5.7% of all ONDI ligands in La-ONDI-DMA, La-ONDI-DMF and La-ONDI-Catechol, respectively.

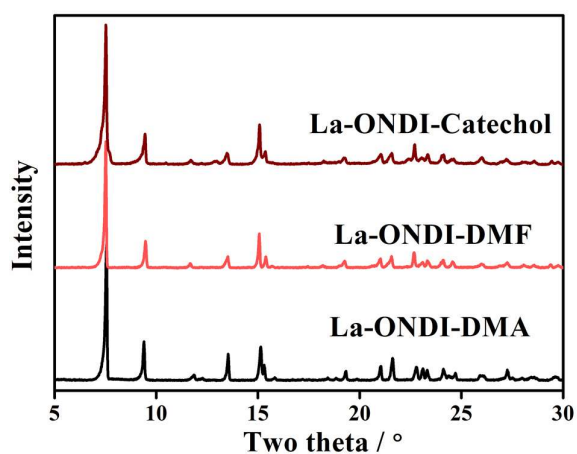


Fig. S13 PXRD patterns of La-ONDI-DMA, La-ONDI-DMF and La-ONDI-Catechol.

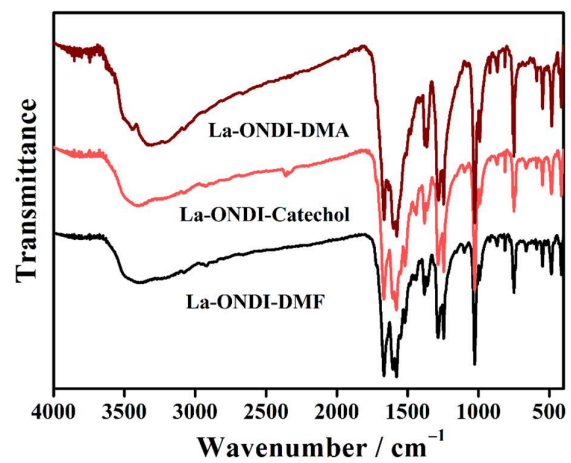


Fig. S14 IR spectra of La-ONDI-DMA, La-ONDI-DMF and La-ONDI-Catechol.

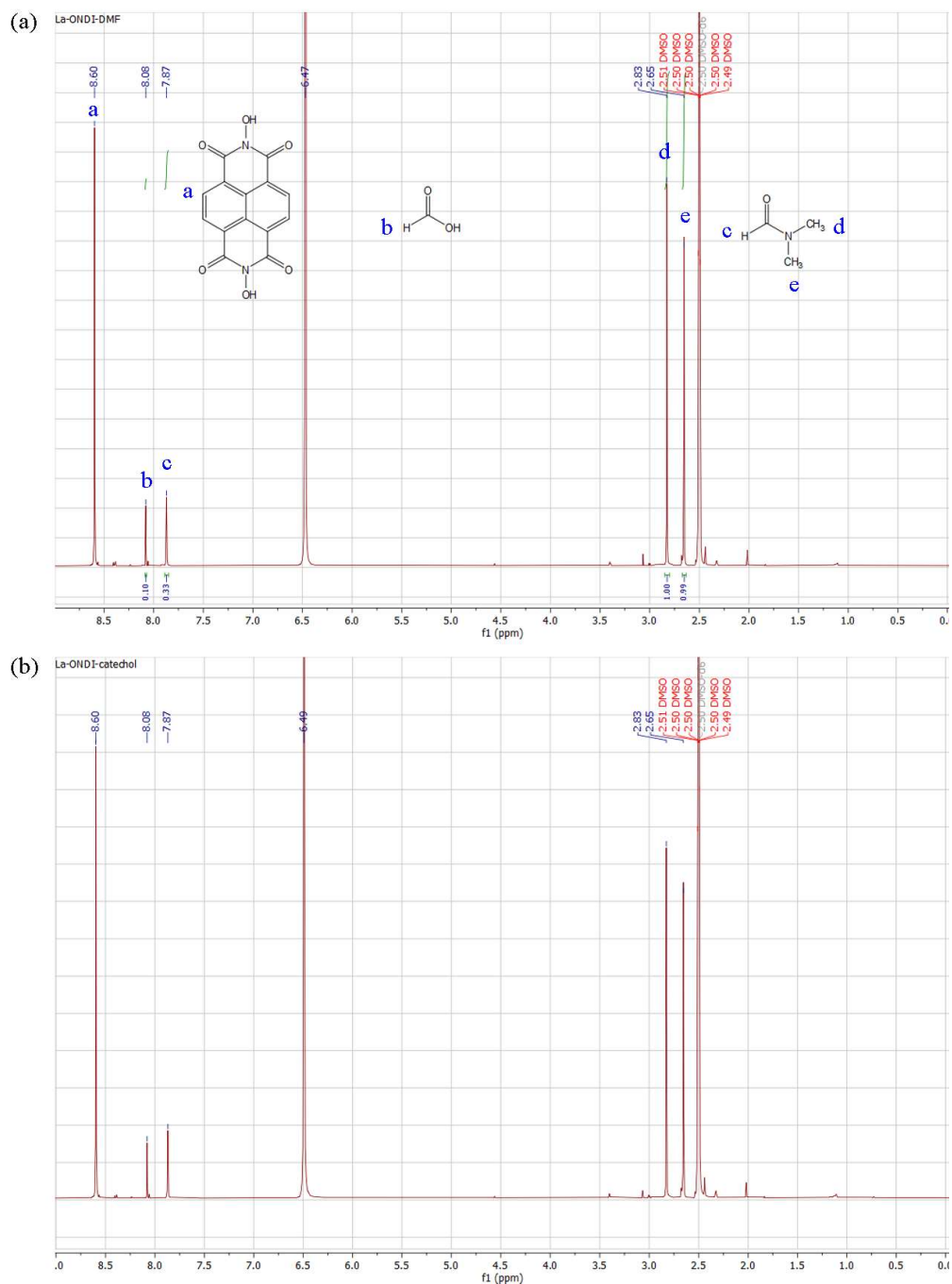


Fig. S15 ¹H NMR spectra of **La-ONDI-DMF** (a) and **La-ONDI-Catechol** (b). The proton signal of formic acid may originate from the hydrolysis of DMF under solvothermal conditions. The proton signals in these two spectra are nearly identical, which indicates that catechol has not been incorporated in **La-ONDI**. These solid samples were dissolved with 0.25 ml DCl (25 wt-% in D₂O) and 1 ml DMSO-d₆. A clear solution was obtained by filtering off (0.45 μm) the yellow precipitate.

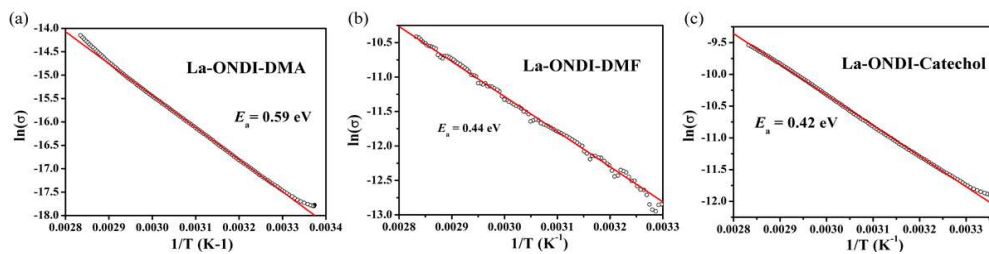


Fig. S16 Temperature dependent electrical conductivity of La-ONDI-DMA, La-ONDI-DMF and La-ONDI-Catechol. The activation energy was estimated based on Arrhenius' equation.

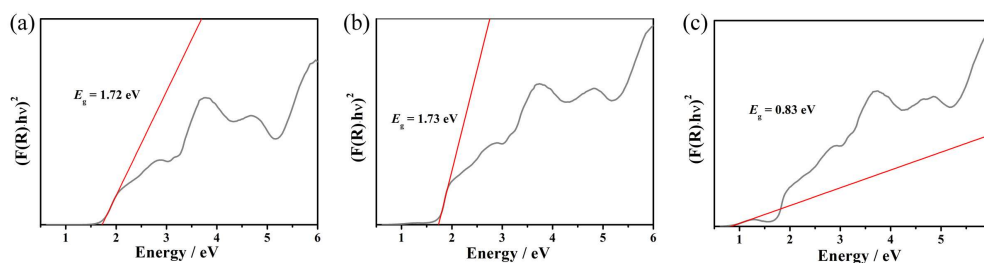


Fig. S17 Tauc plots of La-ONDI-DMA (a), La-ONDI-DMF (b), and La-ONDI-Catechol (c) when regarding them as direct semiconductors.

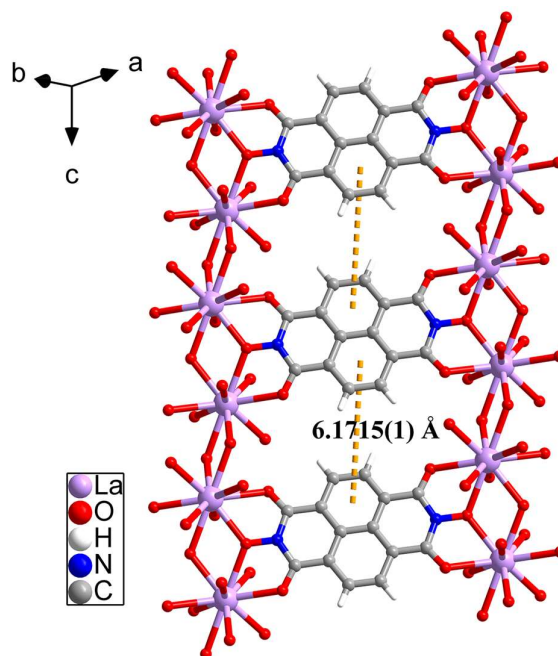


Fig. S18 The ligand arrangement and shortest centroid-centroid distances in La-ONDI.

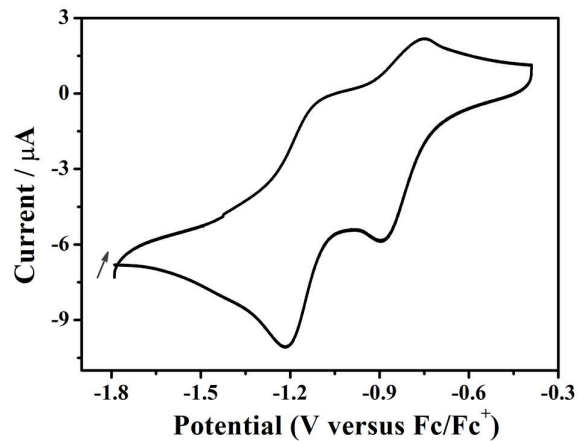


Fig. S19 Solid-state cyclic voltammogram of **La-ONDI**, scan rate 100 mV/s. The redox waves ($E_{1/2} = -1.16$ eV and -0.82 eV) are attributed to ligand-centered redox processes.

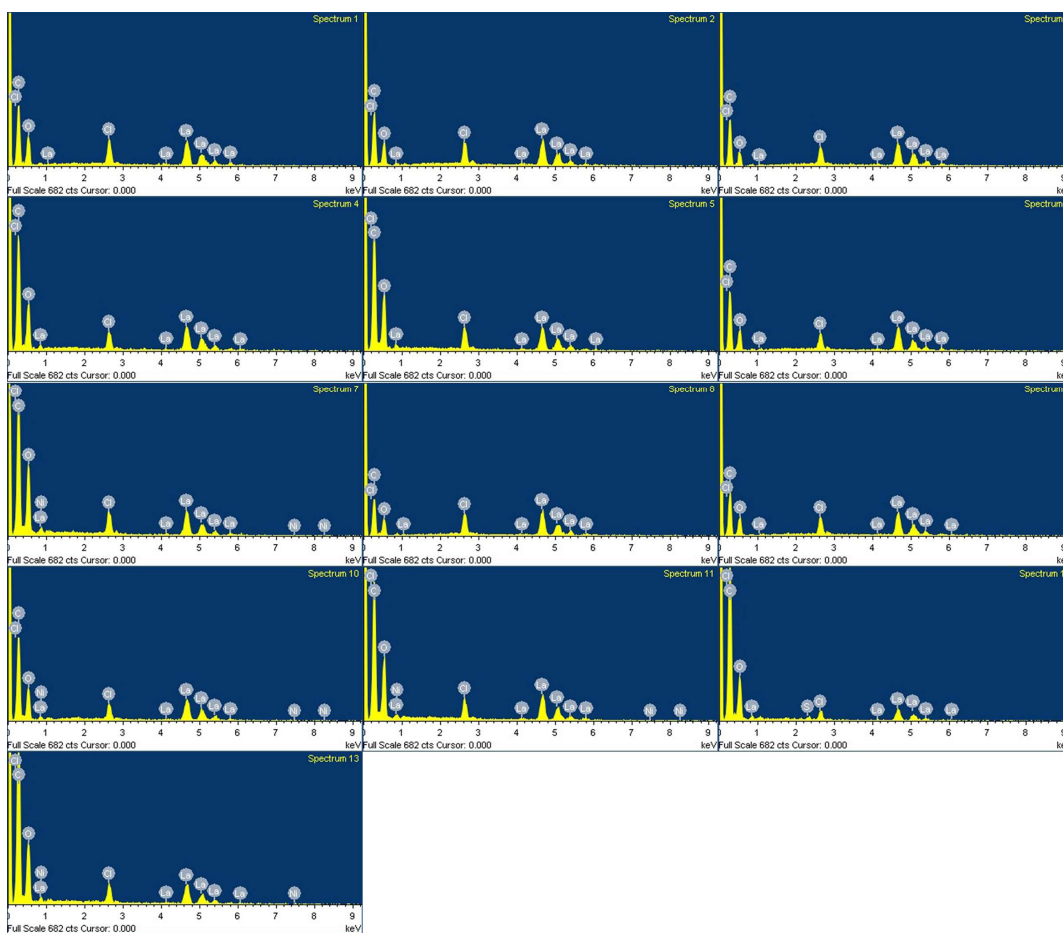


Fig. S20 EDX spectra of **La-ONDI**.

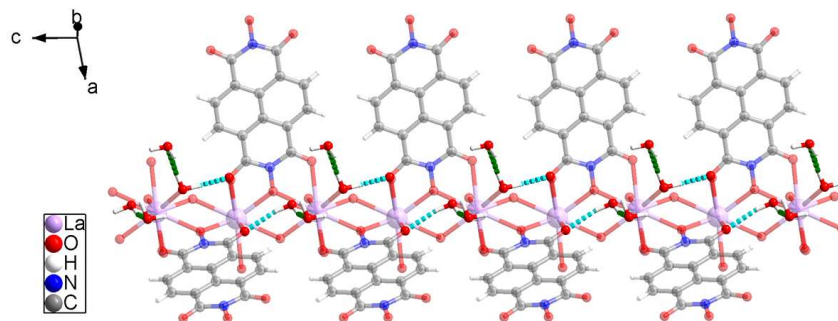


Fig. S21 Hydrogen bonds between water of crystallization and coordinating water molecules. The O...O distances of hydrogen bonds are 2.82(1) Å (green dashed bonds) and 2.932(5) Å (cyan dashed bonds). There is no continuous hydrogen bond network.

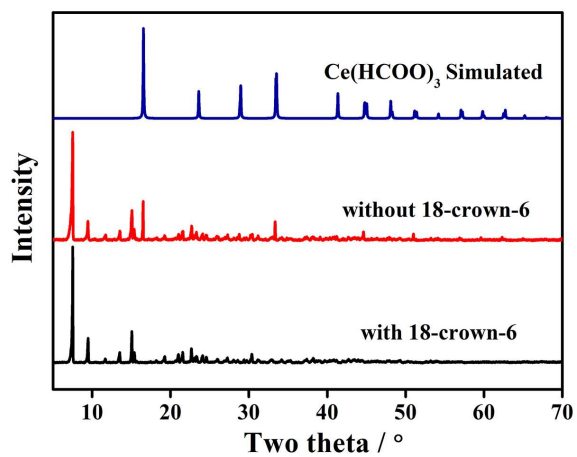


Fig. S22 PXR D patterns of La-ONDI-DMF synthesized in presence of 18-crown-6 (black) and without 18-crown-6 (red), and reported $\text{Ce}(\text{HCOO})_3^5$ (blue). The colorless byproduct is suggested to be $\text{La}(\text{HCOO})_3$.

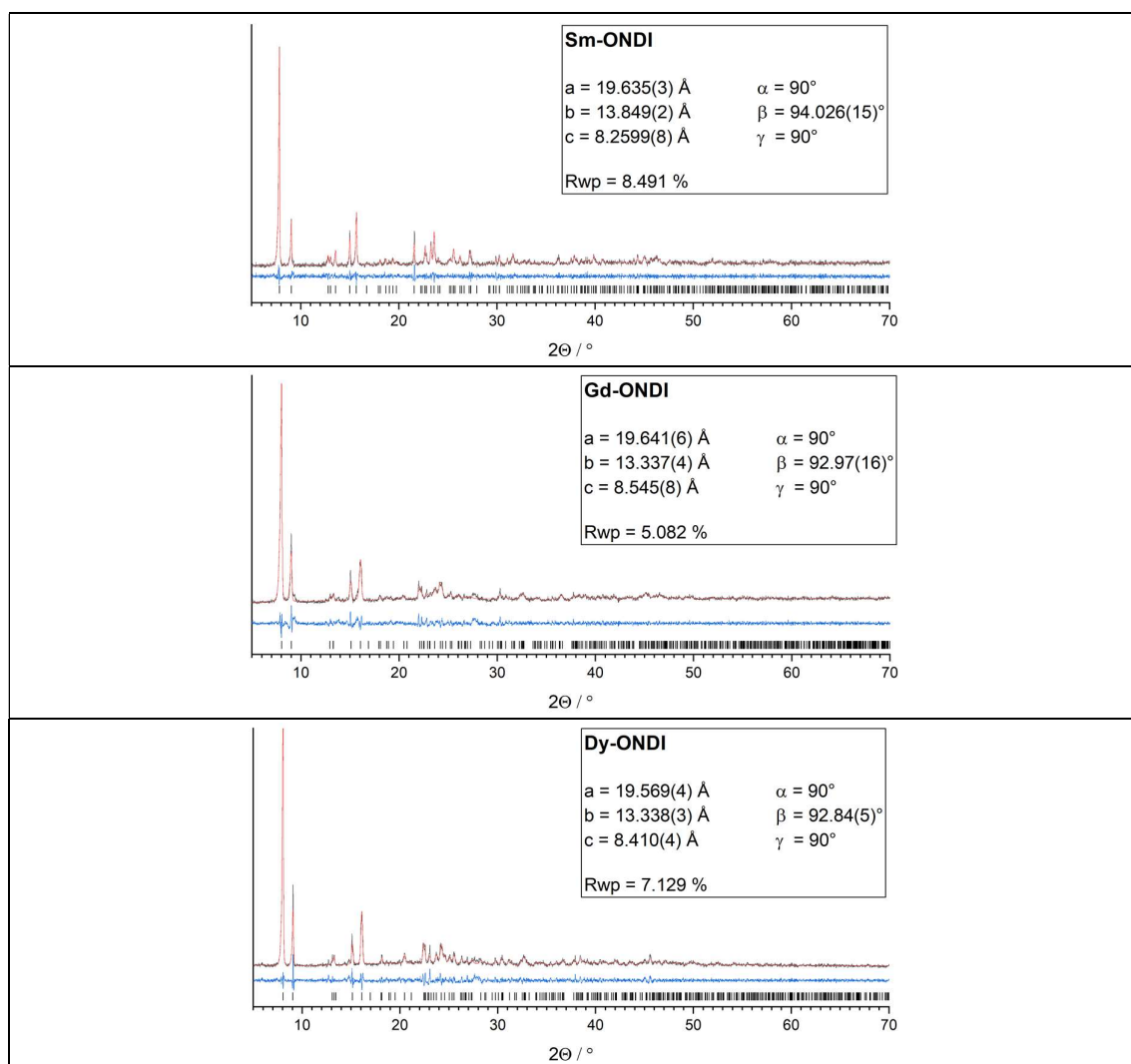


Fig. S23 PXR D patterns and unit cell refinement results of **Sm-ONDI** (a), **Gd-ONDI** (b) and **Dy-ONDI** (c). The Pawley refinement has been performed with the program TOPAS.^[7]

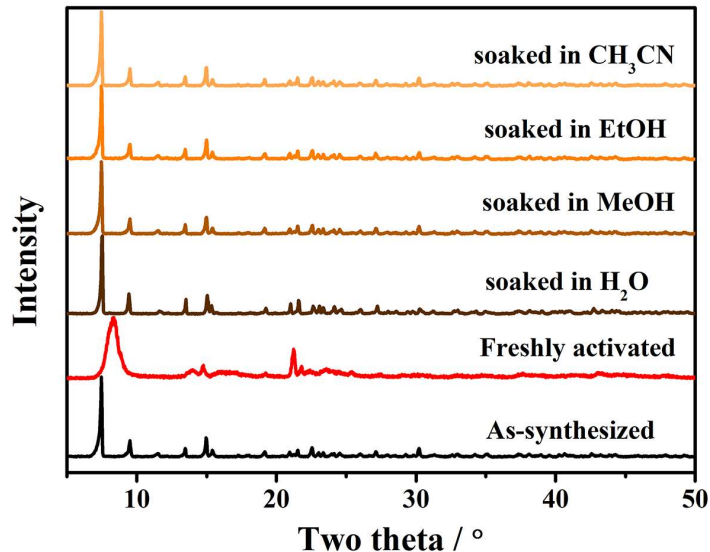


Fig. S24 PXRD patterns of activated **La-ONDI** after soaking in different solvents for 2 days. About 20 mg freshly activated **La-ONDI** was soaked in 2 ml solvent for two days, filtered off and investigated by PXRD.

References:

1. A. L. Spek, *Acta Crystallogr., Sect. C: Struct. Chem.*, 2015, **71**, 9–18.
2. H. C. Wentz, G. Skorupskii, A. B. Bonfim, J. L. Mancuso, C. H. Hendon, E. H. Oriel, G. T. Sazama and M. G. Campbell, *Chem. Sci.*, 2020, **11**, 1342–1346.
3. L. Qu, H. Iguchi, S. Takaishi, F. Habib, C. F. Leong, D. M. D'Alessandro, M. Yamashita, H. Abe, E. Nishibori and M. Yamashita, *J. Am. Chem. Soc.*, 2019, **141**, 6802–6806.
4. K. Fuku, M. Miyata, S. Takaishi, T. Yoshida, M. Yamashita, N. Hoshino, T. Akutagawa, H. Ohtsu, M. Kawano and H. Iguchi, *Chem. Commun.*, 2020, **56**, 8619–8622.
5. C. Hennig, A. Ikeda-Ohno, W. Kraus, S. Weiss, P. Pattison, H. Emerich, P. M. Abdala and A. C. Scheinost, *Inorg. Chem.*, 2013, **52**, 11734–11743.
6. O. V. Dolomanov, L. J. Bourhis, R. J. Gildea, J. A. K. Howard, H. Puschmann, *J. Appl. Cryst.*, 2009, **42**, 339–341.
7. Bruker AXS, *TOPAS Version 5, Karlsruhe*, 2014.